Statistical analysis of the influence of forces on particles in EM driven recirculated turbulent flows

2011 J. Phys.: Conf. Ser. 333 012015

(http://iopscience.iop.org/1742-6596/333/1/012015)

Statistical analysis of the influence of forces on particles in EM driven recirculated turbulent flows

M Ščepanskis[1], A Jakovičs[1] and E Baake[2]

[1] Laboratory for Mathematical Modelling of Environmental and Technological Processes, University of Latvia, 8 Zeļļu str., Rīga, LV-1002, Latvia
[2] Institute of Electrotechnology, Leibniz University of Hanover, 4 Wilhelm-Busch-str., Hannover, D-30167, Germany

E-mail: mihails.scepanskis@lu.lv

Abstract. The present paper contains an analysis of the statistical distribution of forces affecting non-conducting particles dispersed in an EM induced recirculated flow in induction furnaces. The simulation is conducted adopting the LES-based Euler-Lagrange approach in the limit of dilute conditions (one-way coupling). It is done by means of a development of *OpenFOAM* software code. The used Lagrange equation for particle tracking includes drag, EM, buoyancy, lift, acceleration and added mass forces. The relevant approximations for the forces are chosen on the basis of the statistical analysis of the non-dimensional parameters (particle Reynolds number, shear stress and acceleration parameter). The effect of force distribution on particle homogenization is described under different density ratios and particle sizes. The recommendations of the consistence of the Lagrange model for the simulation of the particle motion in the laboratory scale induction crucible furnace are given in conclusion.

1. Introduction

The present paper deals with the transportation of solid particles in a recirculated flow of metal melt in industrial electroheat equipment. Different types of induction furnaces are used, but all of them have the same physical principle of operation and consequently similar flow distribution in the induction furnaces, e.g. in a vertical cross section of an induction crucible furnace (ICF) [1] and in a cross section of a channel in a channel induction furnace (CIF) [2].

The sketch of an axis-symmetric induction system is shown on the figure 1. Alternating current in the inductor ($\boldsymbol{j}_{\mathsf{I}}$ is the current density) creates a magnetic field $\boldsymbol{B}$ and induces an alternating current in the conductive liquid metal ($\boldsymbol{j}_{\mathsf{B}}$ is the density of the induced current). The directions of $\boldsymbol{j}_{\mathsf{B}}$ and $\boldsymbol{j}_{\mathsf{I}}$ are opposite. The result of the interaction of $\boldsymbol{j}_{\mathsf{B}}$ and $\boldsymbol{B}$ is the Lorentz force, which can be expressed as $\boldsymbol{f}_{\mathsf{em}}(t) = \left[\boldsymbol{j}_{\mathsf{B}} \times \boldsymbol{B}\right]$. This force drives the liquid away from the wall. So far as $\boldsymbol{f}_{\mathsf{Lorentz}}$ has the maximum in the middle zone of the crucible (on the half-height of the inductor), the flow pattern consists of two eddies as it is shown on the figure 1 and in the case of cylindrical 3D geometry it means two toroidal vortices. Generally $\boldsymbol{f}_{\mathsf{em}}(t)$ is harmonic, but as far as the frequency of $\boldsymbol{j}_{\mathsf{I}}$ in the industrial electroheat equipment and density of metal are sufficiently high, the time for the metal to respond on the changes of the current is not enough. Therefore we can replace the harmonic force

density with its average value (hereinafter we will type amplitude of the harmonic variables without any additional symbols):

$$f_{\mathrm{em}} = \frac{1}{2}\left[j_{\mathrm{B}} \times B^{*}\right], \tag{1}$$

where B^{*} is complex conjugated magnetic field induction.

The power of ICFs and CIFs is sufficiently high enough to produce turbulent flow with high Reynolds numbers (e.g. for laboratory ICF it is about 10^5). The flow patterns and the turbulent properties of such systems were studied well experimentally and numerically during the last years (see e.g. [1,3-5]). As it is already discussed above the two toroidal vortices appear in the time averaged case, but in practice at each moment the turbulent flow consists of numerous eddies with different sizes. However, after the initial transition period the common structure of the flow becomes quasistationary (statistically stationary).

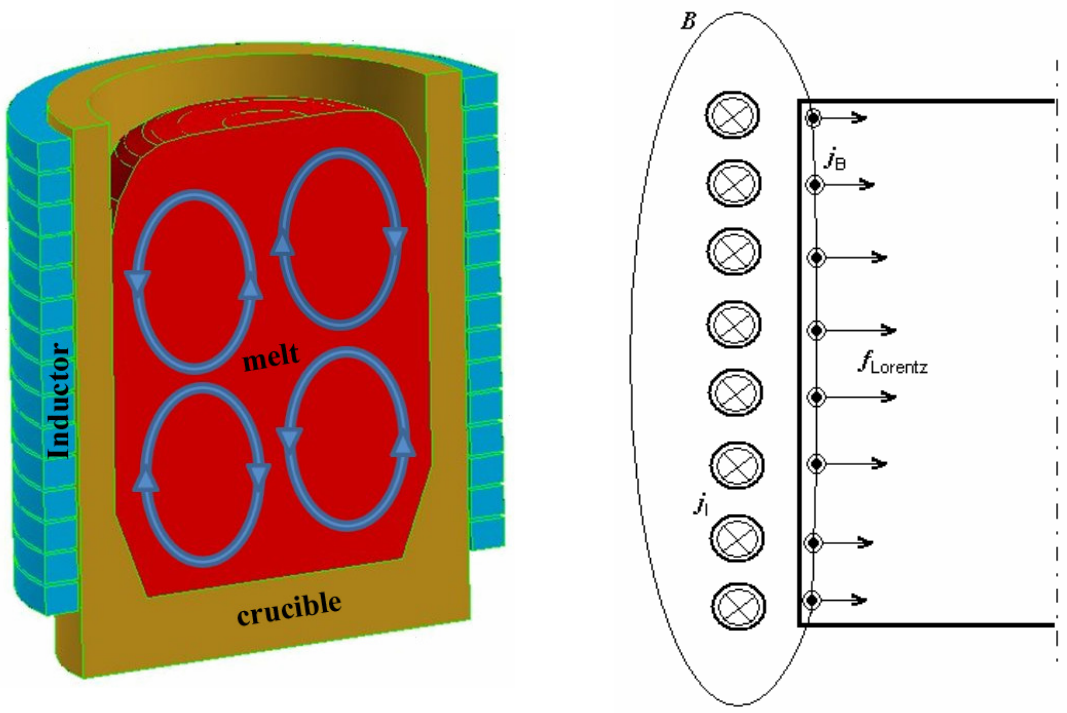

Figure 1. Sketch of axis-symmetric induction system on the example of induction crucible furnace.

The results produced by k-ε turbulence model, with a standard set of constants, show the highest values of turbulent kinetic energy in the eddy centers and the lowest between the eddies. Such distribution is characteristic for the k-ε model even in the case of 3D transient simulation [5]. Experimental results show that the maximum of the turbulent energy is between the vortices of the averaged flow and close to the wall of the crucible [1,5]. The average flow velocity in this area is close to zero, so turbulent pulsations of velocity are large there. It was shown [1,5] that the Large Eddy Simulation (LES) should be used for flow modeling in such equipment to achieve more realistic results. As far as the mass and heat transfer in the zone between the eddies depends on the resolution of the velocity pulsations, the LES has to be used for the objectives of this paper. The spectrum of the pulsations of the axial velocity between these eddies has a clear maximum, which corresponds to the oscillation with a period between 8 and 12 seconds depending on the inductor current [5] (these values are valid only for the particular installation that is simulated also in the present paper).

The flow inside induction furnaces is sufficiently complex due to the presence of the electromagnetic (EM) forces, which drive a turbulent flow with two main toroidal recirculated

vortices. Therefore, the case described in this paper significantly differs from the well-studied turbulence in a pipe, a channel and other classical flows. It also differs from the turbulent flow in the gap between two counterrotating disks (the von Kármán flow) due to intensive axial pulsations between main eddies near the wall [1,5]. Therefore, the behaviour of the particles in such a kind of a flow is interesting from an engineering point of view (see paragraph 1.1) and also is still poor researched (see paragraph 1.2). Moreover, the EM field directly influences the non-conducting particles in the conducting liquid within the penetration depth and transport them to the wall, which is another specific aspect of considered system. The layer of significant EM field is sufficiently thin (about 20% of the radius of the crucible). Due to the non-slip boundary conditions the flow velocity is zero at the wall and increases dramatically in a radial direction until it achieves the maximal value. However, this maximum is in flows with high Reynolds numbers inside the layer of EM penetration. Obviously particles preferentially move in the streamline of maximal velocity. Therefore the major part of the particles frequently to the layer of significant EM field. The particle motion in turbulent flows without EM is well researched, but we can not separate the large interior zone without EM field from the thin layer near the wall and should consider the motion of the particles in the whole volume.

1.1. Motivation

EM heating and melting is one of the most effective methods for melting and processing of conducting materials. However there are some problems concerning the deposition of the impurities like dirty secondary metals as well as the erosion of the walls of the crucible. These processes can significantly reduce the efficiency of the equipment up to breakdown (e.g. channel clogging in CIF). This is one of the reasons for studying of the mass transfer processes in electroheat equipment.

In addition there is a problem of the homogenization of alloying particles, which are mixed in a steel melt to improve properties like strength, hardness and wear resistance. It is important to achieve homogeneous admixtures distribution to ensure a high quality of the alloy. Furthermore it is desirable to reduce the time of mixing to decrease the energy consumptions and prevent the melt from overheating. It is possible to investigate the optimal parameters (such as the size of alloying particles, the time of mixing and other parameters) for industrial processes on the basis of the numerical simulation.

The most impurities and alloying elements have higher melting temperatures than metal. Thereby the melt can contain admixtures as solid particles. However, metals often have very high melting temperatures and are not optical transparent. Therefore experimental investigations of particle motion and mass transfer processes are very difficult to achieve.

There is no experimental technique (known by authors) that gives a possibility to study the dynamics of the particle motion inside the melt. The only known method is developed by Taniguchi et al. [6,7], which gives the possibility to investigate experimentally the rate of the particle deposition in a turbulent flow of liquid metal under EM force. However, because the results are obtained by cutting solidified liquid, it is impossible to receive any information about the dynamics of the process inside the melt using such experimental technique. Moreover the presence of the solidification front has an influence on the particles during the solidification and it is not clear, if this effect is negligible.

Generally transparent liquids are poor electrical conductors, so thermal convection dominates in such systems. Therefore they can not be used to produce such flow patterns. On the other hand non-optical particle measurement techniques are not applicable due to the strong EM field around the equipment.

Therefore numerical simulations are an important way to study parameters of induction equipments and to investigate optimal parameters of admixture particles and thereby to improve energy efficiency of melting and homogenization processes. However, because of the absence of the experimental results, the only chance to verify the models is to compare the results with unpublished industrial reports, which contain some qualitative information.

1.2. Previous investigations

Particle behaviour has been widely investigated in turbulence without EM influence (see e.g. [8]). However, the experimental results received by Taniguchi et al. [6,7] show the significant influence of the EM field on the non-conductive particles in well-conductive liquid. In spite of probable inaccuracy of this experimental technique (a doubt about accuracy is already discussed above), the preferential concentration of the non-conductive particles near the wall at the height of the maximum of the EM force (1) corresponds to the industrial observations.

McKee et al. proposed the greatly simplified analytical model for the calculation of the non-conductive particle path in rotating magnetohydrodynamic flow within a long cylinder [9].

Kirpo et al. used Fluent software to investigate the behaviour of the particle cloud in the turbulent flows in induction furnaces [10]. This model was sufficiently rough: only drag, buoyancy and EM forces were taken into account for the calculations of the particle motion. The particles were initially distributed in a vertical plane, but in an industrial process alloying particles are injected on the top surface of the melt. However, general peculiarity of the particle behaviour was confirmed: the big non-conductive particles were settling down on the wall in the zone between the main vortices.

The model used by Kirpo was enchanced by Ščepanskis et al. by means of a development of *OpenFOAM* software code [11]: 1) the initial cloud of the particles was situated on the top surface of the melt, which corresponds to the industrial case of admixture injection, and 2) the Lagrange equation was supplemented with lift, acceleration and added mass forces. The calculations predicted the scheme of the particle motion during the industrial process of the admixture homogenization in the last paper. The general objective of the paper [11] was to investigate numerically process of the homogenization of non-conductive admixture particles in ICF, but not enough attention was paid to the analysis of the significance of all forces in the model. The importance of full set of the forces was proved as the separating trajectories of the particles with equal initial position but different set of forces. However the insignificant shift of the trajectory can lead to the significant changes in turbulent flows. Therefore evidently the statistical analysis of the forces and the non-dimensional parameters, which is done in the present paper, is important to substantiate the model for the particle motion for this industrially essential application.

It was also stated in [11] that the homogenization takes place between the zones of the main vortices and has an oscillating nature. The rate of the homogenization depends on the size and relative density of the particles. It was also observed that the processes, which occur in the middle zone near the wall, define the characteristic type of the particle motion. The balance between EM, drag and buoyancy forces defines the rate of the homogenization. The last paper contains only approximate theoretical analysis of the force influence on the process of homogenization, so it became clear that additional simulations should be carried out to investigate the contribution of different forces to the homogenization process. The present paper contains such results of numerical simulation.

2. Parameters of laboratory scale equipment and the mesh

A cylindrical ICF is a typical object for inductive melting processes. The sketch of an ICF is shown on the figure 1 and its parameters are shown on the table 1.

Table 1. Parameters of the laboratory scale ICF.

Parameter	Value
inductor frequency	365 Hz
inductor effective current	2000 A
melt and inductor height	570 mm
crucible radius	158 mm
gap between crucible and inductor	38.5 mm
number of inductor turns	12

As far as the flow consists of two main toroidal eddies, the size of the main eddy is approximately equal to the radius of the crucible. The calculations show that we have to use at least 5 cells per eddy

to resolve these vortices. To simulate directly the vortices of one order of magnitude smaller we should refine the cells until its linear size meets a size of 3 mm (2% of the size of the main eddy). The size of the elements decreases near the wall (the width of the smallest element is 0.1 mm). The characteristic velocity of the flow in the main eddies is about 0.15 m/s [5], therefore the approximate time of the circulation is about 3.3 s. The LES calculation was carried out using a time step of 5 ms, which is 0.15% of the typical circulation time.

3. Mathematical model

The present model includes the simulation of the flow and the particle motion. The turbulent flow is calculated using the LES method with the isotropic Smagorinsky subgrid viscosity model:

$$\nu_{\mathrm{SGS}} = C_{\mathrm{k}} \cdot \sqrt{k} \cdot \delta, \qquad k = 2\frac{C_{\mathrm{k}}}{C_{\mathrm{e}}} \cdot \delta^2 \cdot \left|D_{ij}\right|^2, \qquad \delta = \sqrt[3]{V_{\mathrm{c}}},$$

where D_{ij} is the deformation tensor, V_{c} is the volume of the computational cell, $C_{\mathrm{k}} = 0.07$ and $C_{\mathrm{e}} = 1.05$. No additional boundary treatment is applied. The slip boundary condition (BC) on the top surface and the non-slip BC on the walls are applied.

The flow is driven by EM force and thermal buoyancy force in the Boussinesq approximation. The thermal BC are convective on the top surface and adiabatic on the walls of the crucible.

At each time step the results of the flow simulation gives the field of flow velocities, which is used for further calculation of the particle trajectories. The Lagrange equation describes the motion of the inertial particles. In the LES framework we know only the filtered velocity and assume the isotropy of the subgrid part. A statistical approach to the analysis of the force distribution will be discussed below. In spite of the calculation of the individual trajectories of particles, the analysis will be done for the cloud, so the unfiltered isotropic part of velocity should not significantly influence the statistical results. As far as the homogenization criterion is also based on the statistics, the subgrid part should not affect the results of the homogenization process too.

3.1. Lagrange equation

Let us first consider a movable spherical particle in a still liquid. If we solve the stationary Navier-Stokes equation, we will obtain the force that acts on the spherical particle (the Stokes force) as follows:

$$\frac{1}{m}\boldsymbol{F} = \frac{18\nu}{d^2}\frac{\rho_{\mathrm{f}}}{\rho_{\mathrm{p}}} \cdot \left(\boldsymbol{u}_{\mathrm{f}} - \boldsymbol{u}_{\mathrm{p}}\right), \tag{2}$$

where m is the mass of the particle, ν is the kinematic viscosity of the liquid, d is a diameter of the particle, ρ_{f} and ρ_{p} are liquid and particle densities respectively, $\boldsymbol{u}_{\mathrm{f}}$ and $\boldsymbol{u}_{\mathrm{p}}$ are fluid and particle velocities respectively. If we solve the non-stationary Navier-Stokes equation, then the force (2) will be generalized by adding the non-stationary terms [12,13]:

$$\frac{1}{m}\boldsymbol{F} = \frac{1}{2}\frac{\rho_{\mathrm{f}}}{\rho_{\mathrm{p}}}\frac{\mathrm{d}\left(\boldsymbol{u}_{\mathrm{f}} - \boldsymbol{u}_{\mathrm{p}}\right)}{\mathrm{d}t} + \frac{\mathrm{d}\boldsymbol{u}_{\mathrm{f}}}{\mathrm{d}t} + \frac{18\nu}{d^2}\frac{\rho_{\mathrm{f}}}{\rho_{\mathrm{p}}} \cdot \left(\boldsymbol{u}_{\mathrm{f}} - \boldsymbol{u}_{\mathrm{p}}\right) + \frac{9}{d} \cdot \left(\frac{\nu}{\pi}\right)^{1/2} \frac{1}{\rho_{\mathrm{p}}} \cdot \int_0^t \frac{\mathrm{d}\left(\boldsymbol{u}_{\mathrm{f}} - \boldsymbol{u}_{\mathrm{p}}\right)}{\mathrm{d}\tau} \frac{\mathrm{d}\tau}{\sqrt{t-\tau}}. \tag{3}$$

We can compare this result to the result obtained for a potential liquid and generalize it by replacing the simple derivation $\mathrm{d}\boldsymbol{u}_{\mathrm{f}}/\mathrm{d}t$ with the material derivation $\mathrm{D}\boldsymbol{u}_{\mathrm{f}}/\mathrm{D}t$ [13,14].

The contribution to the force made by the summand, that contains the integral, is not so significant because of the oscillating flow acceleration [15]. In addition it is complex for numerical modeling and will be neglected.

It is necessary to note that the flow in our case is not the Stokes flow. Therefore the drag coefficient C_{D} [16] should correct the third summand in (3) and the first summand should be multiplied by the acceleration coefficient C_{A} [17]:

$$C_{\mathrm{D}} = \frac{18\nu}{d^2}\frac{\rho_{\mathrm{f}}}{\rho_{\mathrm{p}}}\left(1 + 0.15\cdot \mathrm{Re}_{\mathrm{p}}^{0.687}\right), \qquad C_{\mathrm{A}} = 2.1 - \frac{0.132}{0.12 + Ac^2}, \tag{4}$$

where $\mathrm{Re}_{\mathrm{p}} = dU/\nu$ is the particle Reynolds number, $Ac = U^2 d^{-1}\left(\mathrm{d}U/\mathrm{d}t\right)^{-1}$ is acceleration parameter, $U = u_{\mathrm{f}} - u_{\mathrm{p}}$ is relative particle velocity. It is clear from (4) that if $\mathrm{Re}_{\mathrm{p}} > 1$, than C_{D} should be expressed in Schiller-Naumann form.

As it was mentioned above some additional forces should be taken into account in the Lagrangian equation.

Lift force appears due to the flow circulation around the particle [18]:

$$\frac{1}{m}\boldsymbol{F}_{\mathrm{lift}} = \frac{\rho_f}{\rho_p}\cdot C_{\mathrm{L}}\cdot\left[\boldsymbol{U}\times\left[\nabla\times\boldsymbol{U}\right]\right] \equiv \frac{\rho_f}{\rho_p}\cdot C_{\mathrm{L}}\cdot\boldsymbol{\xi}, \tag{5}$$

where C_{L} is lift coefficient that depends on Re_{p} and non-dimensional shear stress $Sr = \left|\partial \boldsymbol{u}_{\mathrm{f}}/\partial \boldsymbol{s}\right|\cdot d/U$, where $\boldsymbol{s}$ is a unit vector perpendicular to $\boldsymbol{U}$. Legendre & Magnaudet [19] generalized the analysis performed by Saffman [20] and McLaughlin [21] for the flows with the low particle Reynolds number, and C_{L} can be approximated as follows (the Saffman approximation) [18,19,21]:

$$C_{\mathrm{L}}^{\mathrm{low\,Re}}(\mathrm{Re}_{\mathrm{p}}, Sr) = \frac{6}{\pi^2}\frac{1}{\sqrt{\mathrm{Re}_{\mathrm{p}}\cdot Sr}}J^{'}(\varepsilon), \qquad J^{'}(\varepsilon) = \frac{J(\infty)}{\left(1 + 0.2\cdot\varepsilon^{-2}\right)^{3/2}}, \qquad \varepsilon = \left(\frac{Sr}{\mathrm{Re}_{\mathrm{p}}}\right)^{1/2},$$

where $J(\infty) = 2.255$. This approximation is also known as the Saffman force. Legendre & Magnaudet propose following approximation for the high particle Reynolds numbers [18]:

$$C_{\mathrm{L}}^{\mathrm{high\,Re}}(\mathrm{Re}_{\mathrm{p}}) = \frac{1}{2}\frac{1 + 16\cdot\mathrm{Re}_{\mathrm{p}}^{-1}}{1 + 29\cdot\mathrm{Re}_{\mathrm{p}}^{-1}}.$$

For the particle Reynolds number between the approximation (McLaughlin-Legendre-Magnaudet) is as follows [18]:

$$C_{\mathrm{L}}(\mathrm{Re}_{\mathrm{p}}, Sr) = \left(\left(C_{\mathrm{L}}^{\mathrm{low\,Re}}(\mathrm{Re}_{\mathrm{p}}, Sr)\right)^2 + \left(C_{\mathrm{L}}^{\mathrm{high\,Re}}(\mathrm{Re}_{\mathrm{p}})\right)^2\right)^{1/2}. \tag{6}$$

As far as C_{L} depends on two parameters (Re_{p} and Sr), it is useful to plot down these dependences (figure 2). The range of Re_{p} and Sr for the particular case will be obtained below and the suitable approximation will be chosen.

The densities ρ_{p} and ρ_{f} are different, so we have to take into account the buoyancy force. As it was mentioned above we should also include the EM force in the equation. A great transition resistance appears on the surface between the particles and the metal, hence, we can consider force acting on the non-conducting particles, which can be expressed as follows [22]:

$$\frac{1}{m}\boldsymbol{F}_{\mathrm{em}} = -\frac{3}{4}\frac{1}{\rho_{\mathrm{p}}}\boldsymbol{f}_{\mathrm{em}}.$$

Thus taking into account all above-mentioned forces, the following Lagrange equation for the non-conductive spherical particle motion is used:

$$\underbrace{\left(1 + \frac{C_{\mathrm{A}}}{2}\frac{\rho_{\mathrm{f}}}{\rho_{\mathrm{p}}}\right)\cdot\frac{\mathrm{d}\boldsymbol{u}_{\mathrm{p}}}{\mathrm{d}t}}_{\mathrm{d}\boldsymbol{u}_{\mathrm{p}}/\mathrm{d}t + \text{added mass force}} = \underbrace{C_{\mathrm{D}}\cdot\boldsymbol{U}}_{\text{drag force}} + \underbrace{\left(1 - \frac{\rho_{\mathrm{f}}}{\rho_{\mathrm{p}}}\right)\cdot\boldsymbol{g}}_{\text{buoyancy force}} - \underbrace{\frac{3}{4}\frac{1}{\rho_{\mathrm{p}}}\boldsymbol{f}_{\mathrm{em}}}_{\text{EM force}} + \underbrace{\frac{\rho_{\mathrm{f}}}{\rho_{\mathrm{p}}}C_{\mathrm{L}}\boldsymbol{\xi}}_{\text{lift force}} + \underbrace{\left(1 + \frac{C_{\mathrm{A}}}{2}\frac{\rho_{\mathrm{f}}}{\rho_{\mathrm{p}}}\right)\cdot\frac{\mathrm{D}\boldsymbol{u}_{\mathrm{f}}}{\mathrm{D}t}}_{\text{acceleration + added mass}},$$

where vector $\boldsymbol{\xi}$ is defined in (5).

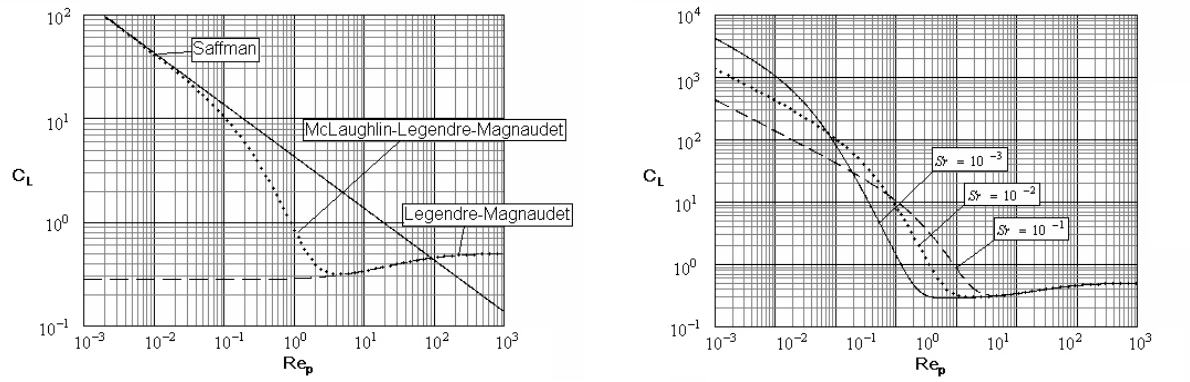

(a) (b)

Figure 2. (a) Different approximations for the lift coefficient C_L (here $Sr = 0.1$); (b) McLaughlin-Legendre-Magnaudet approximation for lift coefficient C_L for different Sr.

We assume that the particle-particle interaction is negligible and the particles do not affect the pattern and the velocities of the flow. This assumption is possible because the volume of the particles do not exceed 1% of the liquid volume.

The particle tracking library in *OpenFOAM* software is supplemented with EM, lift, acceleration and added mass forces. Thereby the Lagrange equation becomes non-linear. To ensure the convergence the hydrodynamic time step was split into various Lagrange time steps (LTS). The non-linear factors in the Lagrange equation are approximated with the values that correspond to the previous LTS (Pikar's method). The implicit scheme is used to solve the equation.

3.2. Particle collision with the wall

The standard *OpenFOAM* algorithm simulates a particle collision with the wall as follows:

$$u_p^{n\,\prime} = \varepsilon \cdot u_p^n,$$

$$u_p^{t\,\prime} = (1-\mu) \cdot u_p^t,$$

where u_p^n and u_p^t are normal and tangential components of the particle velocity before collision; $u_p^{n\,\prime}$ and $u_p^{t\,\prime}$ are normal and tangential components of the particle velocity after collision; The coefficients of restitution and friction have been set to $\varepsilon = 0.8$ and $\mu = 0.2$ in the present simulation.

However the *OpenFOAM* algorithm does not take into account the collision of a particle with the wall in a situation when the size of the particle is larger than the size of a mesh element. If the distance between the particle center and the wall is smaller than the radius, than the present model moves the particle to the distance of the radius from the wall at the end of the each LTS.

4. Statistical analysis of the forces

Particles with a diameter less than 300 μm are well admixed in the melt of the laboratory scale ICF (the parameters of the furnace are shown on the table 1), but larger particles conglomerate at the wall in the middle zone of the crucible due to relative increase of EM force per particle mass unit. It should be underlined that this limit in a particle size and following results are relevant only for ICF of the mentioned laboratory scale, while the obtained dependences should be universal. Mentioned effect can be prevented by increasing the flow velocity (see theoretical investigation in [11]). It is also clear that the size of the main eddies influences the balance of the forces in the middle zone. If the linear velocity of the circular motion is invariable, than the greater is the area of the vortex and the lower is the affect of centrifuging the light particles to the center of the eddy [8]. Therefore the EM force, which moves the particles to the wall, will be more competitive with respect to the centrifuging effect for the large vortices. The ratio of the liquid and particle densities $S = \rho_f / \rho_p$ affects the particle

motion likewise through the EM/centrifuging balance. The dependence of the flow velocity on inductor current and frequency is also known [1]. Apparently there are a lot of dimensional parameters, an attempt to create a composite non-dimensional parameter was not successful. The EM parameters and geometry of the equipment are fixed in the present paper, subsequently the size of the main eddies and the characteristic velocity are also defined; the purpose of the paper is to investigate the dependence on the particle size and their density of the distribution of the forces in ICF of such laboratory scale.

The aim of the following paragraphs is to determine the distribution of the forces that has influence on the particles with different sizes and densities in whole volume. We inject 75 particles in a horizontal plane near the top surface of the crucible. During the period of 10 s the initial cloud of the particles is distributed more or less homogeneous inside the zones of the main vortices (see figure 1), but the number of particles is different between the zones of the upper and the lower main eddies [11]. So we skip this transitional period and start to collect data after that. The values of non-dimensional parameters and the magnitude of the forces are saved for each particle every 50 ms for a period of 20 s, which corresponds approximately to 6 periods of a particle circulation in the main vortex. Therefore the statistical database consists of 75 x 20 / 0.05 = 30000 information units. Thereby we assume that we collect the data from the whole volume and for all states of quasistationary turbulence.

First the statistical analysis of the non-dimensional parameters ($\mathrm{Re_p}$, Sr and Ac) will be done to choose the approximation of the forces. Then the distribution of the force densities will be evaluated.

The particles with the liquid-to-particle density ratio $S = \rho_\mathrm{f}/\rho_\mathrm{p}$ equal to 1 and 1.5 and the diameter d from 10 μm to 200 μm (that is from 6 ppm to 0.1% of the radius of the main vortex) are analyzed.

4.1. Non-dimensional parameters and approximation of the forces

The acceleration parameter $Ac = U^2 d^{-1}(\mathrm{d}U/\mathrm{d}t)^{-1}$ for all examined cases is between 10^2 and 10^5. Thereby the acceleration coefficient (4) can be simply approximated as $C_\mathrm{A} = 2.1$.

The half width of the calculated statistical distribution of the particle Reynolds number $\mathrm{Re_p} = dU/\nu$ is shown on the figure 3. We can see, that the distribution of $\mathrm{Re_p}$ is more or less invariable for the particles with a density equal to the liquid density (figure 3b), except particles with

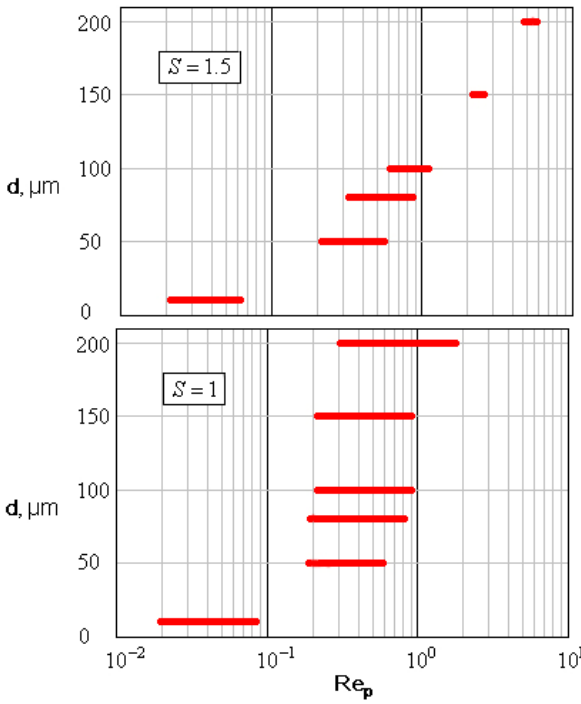

Figure 3. The half width of the calculated statistical distribution of $\mathrm{Re_p}$. (a) $S = \rho_\mathrm{f}/\rho_\mathrm{p} = 1.5$; (b) $S = 1$.

small diameter - 10 μm. For the particles with $S = 1.5$ $\mathrm{Re_p}$ increases with the particle increase in the size. This increase is connected with the significant role of buoyancy force that produces an axial velocity and will be explained below. For $S = 1.5$ and $d > 100\,\mu\mathrm{m}$ $\mathrm{Re_p} > 1$, therefore the Schiller-Naumann approximation (4) for drag coefficient should be used, in other cases the Stokes form for C_D is applicable.

The calculations show that the non-dimensional shear stress Sr varies between 10^{-3} and 10^{-1}. Taking also into account the figure 3 and the behaviour of the lift coefficient (figure 2), we can conclude that C_L should be defined within the McLaughlin-Legendre-Magnaudet approximation (6).

4.2. Forces

Apparently EM force is localized near the wall due to the limited penetration depth of the EM field. Therefore there is no reason to investigate this force statistically.

The half width of the statistical distribution of drag, lift, acceleration and added mass force densities for the particles with the diameters from 10 μm to 200 μm and $S = 1;1.5$ is shown on the figure 4. The mentioned densities approximately correspond e.g. to the densities of steel – niobium and steel – grey tin alloys respectively.

We can notice that added mass and acceleration force densities are relatively independent of the particle size in the both cases ($S = 1$ and $S = 1.5$). On the other hand, the lift force density decreases with the increase of the particle size. The behaviour of drag force density is different for various S. It decreases with the decrease of the particle diameter like the lift force density for the case $S = 1$. But in the case $S = 1.5$ drag force density decreases only until it achieves the value of buoyancy force density, and then it still remains distributed approximately around the buoyancy force point. The buoyancy leads to the axial motion and moves the particles to the surface. In the most cases the drag force opposes the buoyancy and mixes the particle deeper in the melt (e.g. in the zone of the upper eddy near the wall). As far as the drag coefficient C_D decreases with an increase of the particle size (4), buoyancy force and axial motion become relatively stronger for the larger particles. So the particles axial velocity increases and consequently the difference between the flow and particle velocities $\boldsymbol{U} = \boldsymbol{u}_\mathrm{f} - \boldsymbol{u}_\mathrm{p}$ also increases. Thereby we can observe such a coupling of the drag and buoyancy force for the big light particles.

Figure 4 shows that for the particles with $d \geq 80\,\mu\mathrm{m}$ and $S = 1$ we should take into account all forces, but for $d < 80\,\mu\mathrm{m}$ only drag and lift forces. For the particles with $S = 1.5$ and $d \leq 100\,\mu\mathrm{m}$ drag, lift and buoyancy forces should be taken into account, but for the particles with $d \geq 150\,\mu\mathrm{m}$ only drag and buoyancy forces dominate. So we find for the separating size: $d = 80\,\mu\mathrm{m}$ for $S = 1$ and $d = 100\,\mu\mathrm{m}$ for $S = 1.5$. These values separate the sizes, when different sets of forces are applicable. Apparently the separating size for $S > 1$ rises with an increase of S.

Generally the significance of acceleration and added mass forces decreases with the increase of S. The lift force also becomes unimportant for big particles. These regularities should be true also for such systems with the different parameters.

5. Modelling of particle homogenization

After the statistical estimation of the force distribution in the flow of the laboratory scale ICF is done, it is interesting to analyze their influence on the macroscopic particle transportation process such as the process of the alloying particle homogenization in ICF. Generally the homogenization process is already described in [11], but the aim of this paragraph is to study the influence of the different forces on the particle distribution during the homogenization process. Apparently the theoretical analysis of the particle behaviour in the middle zone of the crucible [11] is not enough to understand the role of

the forces during this process. Thereby the simulations with different sets of forces were carried out and the results are discussed below.

Like it was done in [11], the homogenization process in the present paper is analyzed by plotting the values of $\Delta N/N$, where ΔN is the difference between the number of the particles in the zones of the upper and the lower eddies (see figure 5) and N is the number of the particles in the both zones. The magnitude of the average axial velocity is low in the middle zone of the crucible near the wall, but the turbulent pulsations have a maximum between the eddies [1]. Thus the intensive turbulent

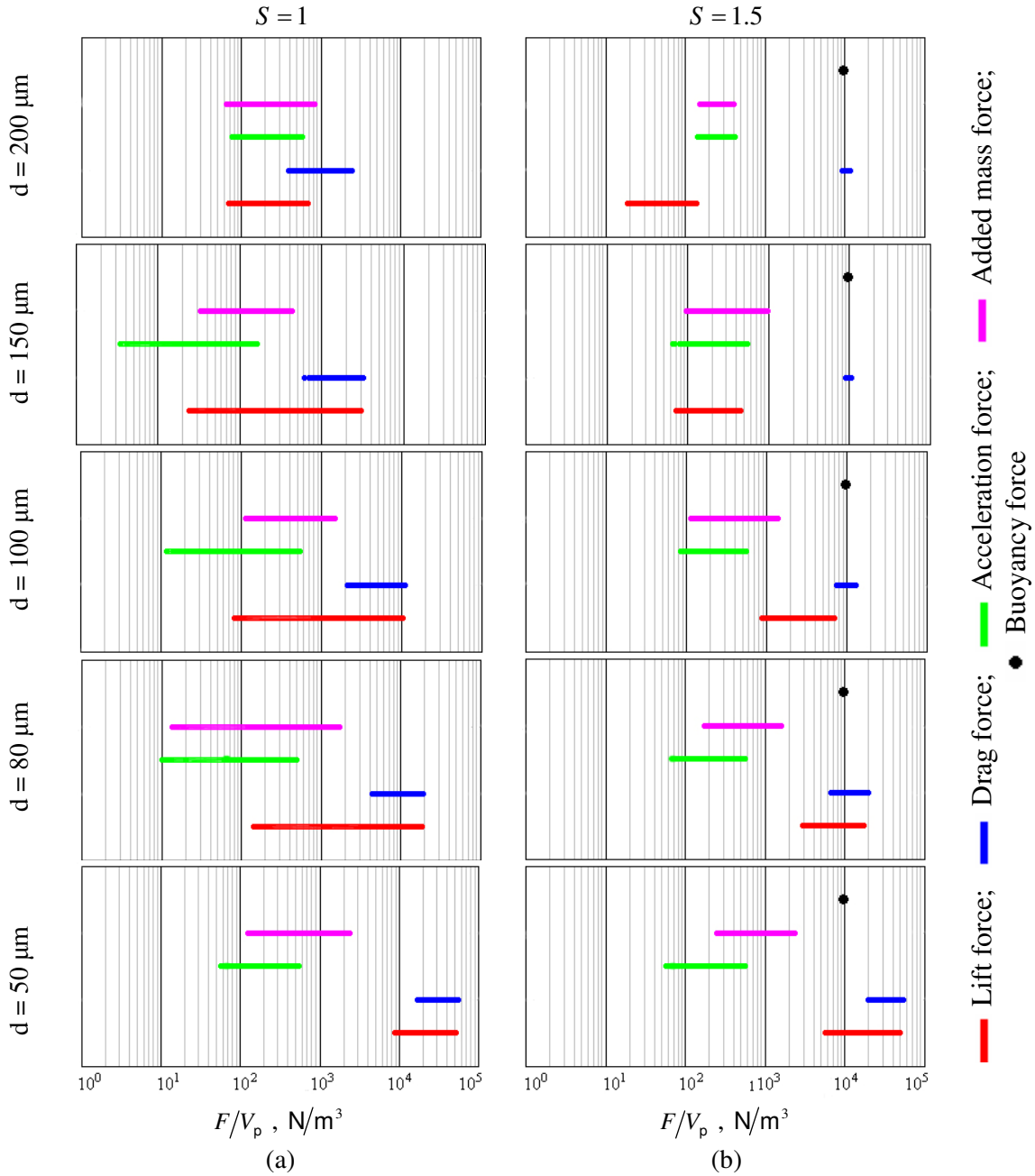

Figure 4. The half width of the calculated statistical distribution of the drag, lift, acceleration and added mass force densities F/V_p, where V_p is particle volume, for the particles with (a) $S = \rho_f/\rho_p = 1$, (b) $S = 1.5$.

pulsations in this area improve the particle exchange and the decrease of ΔN. The results of the simulation show that the radial and the angular distributions of the particles inside the crucible rapidly homogenize (except the thin layer near the wall). Therefore $\Delta N/N$ parameter was chosen for the analysis of the homogenization process.

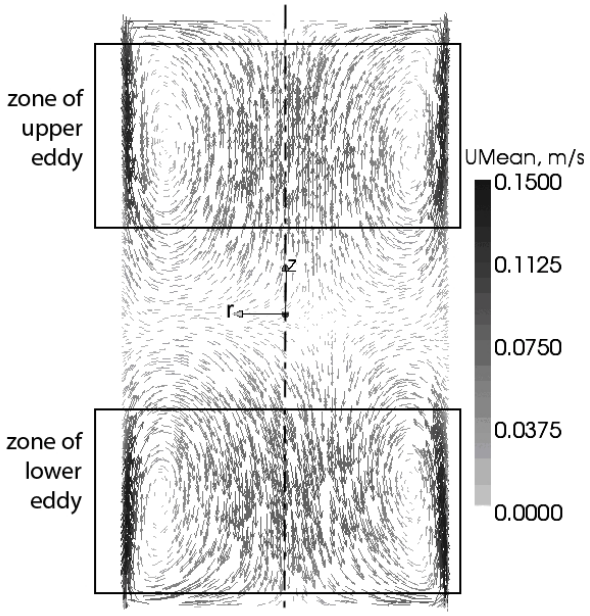

Figure 5. Average flow velocity in the central vertical plane in the ICF. The frames show the zones of the upper and the lower eddies. [11]

It has been already discussed [11] that in spite of the quasistationary flow pattern, the behaviour of the homogenization factor $\Delta N/N$ in time is not quasistationary, but it monotonously decreases. The exchange of the particles between the eddies takes place due to the axial flow pulsations. So each particle in the zone of the upper eddy can reach the lower eddy in only one time per period of the main circle motion. Consequently the process of homogenization is connected with the period of the particle circulation which is approximately 3.3 s (see paragraph 2). The figure 6 illustrates the process of the homogenization during the period of 50 s. It means that the period of the monotonous homogenization on the figure 6 is about 40 s (first 10 s can be counted out as the transitional period), that is about 12 periods of the main circular motion. $\Delta N/N$ tends asymptotically to a constant value which is zero for the case $S=1$ and to some positive value if $S>1$ [11]. $\Delta N/N$ reaches the asymptotic value in approximately 55 s if $S=1$ and in 75 s if $S=1.5$ [11]. However, the figure 6 shows that the absence of some forces in the model leads to a shift of the curve of $\Delta N/N$ and consequently to the misrepresentation of the time for achieving the asymptotic value.

We can see that for the particles with $d=50\,\mu\text{m}$ the difference between the curves that corresponds to the diverse sets of the forces is not so significant. On the contrary the curves for $d=100\,\mu\text{m}$ show a significant divergence. The largest divergence is between the curve that takes into account all forces and the curve without acceleration and added mass forces. This difference increases with an increase of the particle size and leads to a time delay in the process of the homogenization. At the initial moment, when the unmovable particle cloud should be accelerated, acceleration and added mass forces play a great role. Therefore the process of the homogenization is slower without acceleration and added mass forces. The absence of lift force also changes the curve but in the contrast with acceleration forces, it speeds up the homogenization. The divergence between the curve without lift force and the curve with all forces decreases with an increase of S.

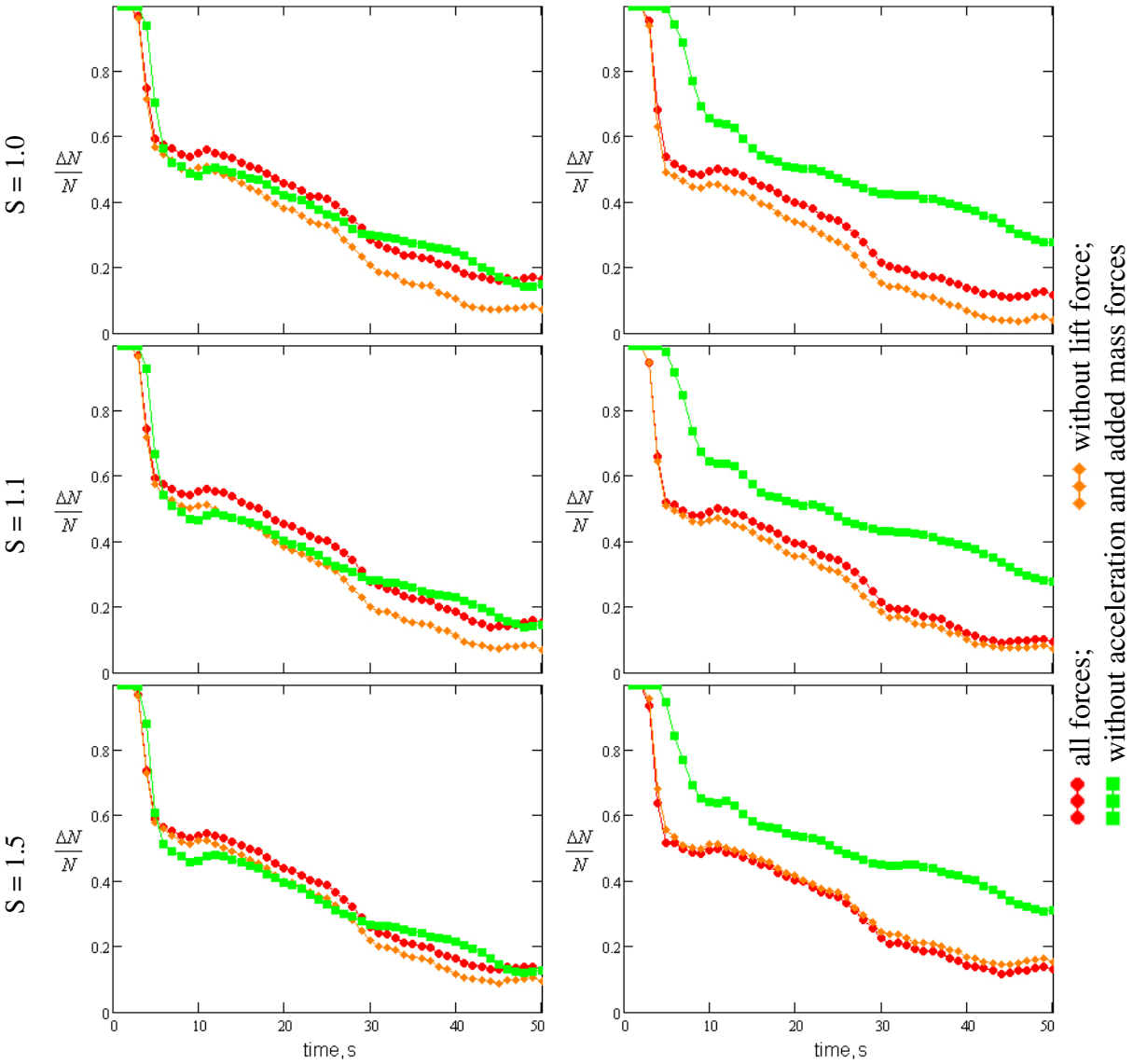

d = 50 μm (a) d = 100 μm (b)

Figure 6. The difference between the number of particles in the zones of the upper and the lower eddies normalized with the respect to the number of the particles in the both zones $\Delta N/N$. (a) $d = 50\,\mu\text{m}$, (b) $d = 100\,\mu\text{m}$

So the simulation of the homogenization process shows that the absence of the forces in the Lagrange model also influences the process of the redistribution of the particles in the volume of the recirculated flow. And the separating values of the particle size for the significance of the forces are approximately equal to the separating values discovered in the paragraph 4.2.

6. Conclusions

The analysis of the significance of the different forces in the Lagrange equation for particle motion and the homogenization process is done in this paper on the basis of the statistical research. The present work proves the significance of drag, lift, EM, acceleration and added mass forces and forms the Lagrange equation that should be used for modelling of the particle transfer in the flow inside an ICF. However in the particular cases of a laboratory scale ICF we can use the short list of the forces:

$S = \rho_f / \rho_p = 1$, $d < 80\,\mu m$ - drag, lift and EM forces;

$S = 1.5$, $d \le 100\,\mu m$ - drag, lift, buoyancy and EM forces;

$S = 1.5$, $d > 100\,\mu m$ - drag, buoyancy and EM forces.

Generally the significance of acceleration and added mass forces decreases with an increase of S. Lift force also becomes unimportant for large particles. The Schiller-Naumann approximation for the drag coefficient, the McLaughlin-Legendre-Magnaudet approximation for lift force and the extreme case of the Odar-Hamilton approximation for the acceleration coefficient should be chosen in the Lagrange equation.

The presence of these forces is also important for the simulation of the homogenization process. The absence of acceleration and added mass forces increases significantly the homogenization time for particles with $d > 50\,\mu m$. The presence of lift force becomes important when $S \approx 1$.

In spite of the particular relevance of the recommendations above (valid only for a laboratory scale ICF), the general dependences should be similar for different parameters of ICFs. Moreover the authors hope that the present recommendations for the Lagrange model will be useful in the engineering studies.

7. Acknowledgement

This work has been partly supported by the European Social Fund within the project «Support for Doctoral Studies at University of Latvia».

References

[1] Kirpo M, Jakovičs A, Baake E and Nacke B 2007 Analysis of experimental and simulation data for the liquid metal flow in a cylindrical vessel *Magnetohydrodynamics* **43** 161-72

[2] Baake E, Jakovičs A, Pavlovs S and Kirpo M 2010 Long-term computations of turbulent flow and temperature field in the induction channel furnace with various channel design *Magnetohydrodynamics* **46** 461-74

[3] El-Kaddah N, Szekeley J, Taberlet E and Fautrelle Y 1986 Turbulent recirculating flow in induction furnaces: a comparison of measurements with predictions over a range of operating conditions *Metallurgical Transactions B* **17B** 687-93

[4] Bojarevics A, Bojarevics V, Gelfgat Yu M and Pericleous K 1999 Liquid metal turbulent flow dynamics in a cylindrical container with free surface: experiment and numerical analysis *Magnetohydrodynamics* **35** 205-22

[5] Umbrashko A, Baake E, Nacke B and Jakovics A 2006 Modeling of the turbulent flow in induction furnaces *Metallurgical and Materials Transactions B* **37B** 831-8

[6] Taniguchi S and Brimacombe J K 1994 Application of pinch force to the separation of inclusion particles from liquid steel *ISIJ International* **34** 722-31

[7] Takahashi K and Taniguchi S 2003 Electromagnetic separation of non-metallic inclusion from liquid metal by imposition of high frequency magnetic field *ISIJ International* **43** 820-7

[8] Toschi F and Bodenschatz E 2009 Lagrangian properties of particles in turbulence *Annu. Rev. Fluid Mech.* **41** 375-404

[9] McKee S, Watson R, Cuminato J R and Moor P 1999 Particle-tracking within-turbulent cylindrical electromagnetically-driven flow *Int. J. Numer. Meth. Fluids* **29** 59-74

[10] Kirpo M, Jakovičs A, Baake E and Nacke B 2009 LES study of particle transport in turbulent recirculated liquid metal flows *Magnetohydrodynamics* **45** 439-50

[11] Ščepanskis M, Jakovičs A and Nacke B 2010 Homogenization of non-conductive particles in EM induced metal flow in a cylindrical vessel *Magnetohydrodynamics* **46** 413-23

[12] Basset A B 1888 *A treatise on hydrodynamics with numerous examples* vol 2 (Cambridge: Deighton, Bell and Co)

[13] Brennen C E 2005 *Fundumentals of multiphase flow* (New York: Cambridge University Press)

[14] Crowe C T, Sommerfeld M and Tsuji Y 1998 *Multiphase flows with droplets and particles*

(Boca Raton, Florida: CRC Press)
[15] Kirpo M, Jakovičs A, Baake E and Nacke B 2006 Modeling velocity pulsations in a turbulent recirculated melt flow *Magnetohydrodynamics* **42** 207-18
[16] Schiller L and Naumann Z 1933 Uber die grundlegenden Berechnungen bei der Schwerkrafttaufbereitung (in German) *Ver. Deut. Ing.* **77** 318-20
[17] Odar F and Hamilton W S 1964 Forces on a sphere accelerating in a viscous fluid *J. Fluid Mech.* **18** 302-14
[18] Legendre D and Magnaudet J 1998 The lift force on a spherical bubble in a viscous linear shear flow *J. Fluid Mech.* **368** 81-126
[19] Legendre D and Magnaudet J 1997 A note on the lift force on a bubble or a drop in a low-Reynolds-number shear flow *Phys. Fluids* **9** 3572-4
[20] Saffman P G 1965 The lift on a small sphere in a slow shear flow *J. Fluid Mech.* **22** 385-400
[21] McLaughlin J B 1991 Inertial migration of small sphere in linear shear flows *J. Fluid Mech.* **224** 261-74
[22] Leenov D and Kolin A 1954 Theory of electromagnetophoresis I Magnetohydrodynamic forces experienced by spherical and symmetrically oriented cylindrical particles *J. of Chem. Phys.* **22** 683-89